Designing Surface Charge Patterns for Shape Control of Deformable Nanoparticles

Nicholas E. Brunk,[1,2] JCS Kadupitiya,[1] and Vikram Jadhao[1,*]
[1]Intelligent Systems Engineering, Indiana University, Bloomington, Indiana 47408, USA
[2]Wolfram Research, Champaign, Illinois 61820, USA

(Received 12 July 2020; revised 9 October 2020; accepted 12 November 2020; published 10 December 2020)

Designing reconfigurable materials based on deformable nanoparticles (NPs) hinges on an understanding of the energetically favored shapes these NPs can adopt. Using simulations, we show that hollow, deformable, patchy NPs tailored with surface charge patterns such as Janus patches, stripes, and polyhedrally distributed patches differently adapt their shape in response to changes in patterns and ionic strength, transforming into capsules, hemispheres, variably dimpled bowls, and polyhedra. The links between anisotropy in NP surface charge, shape, and the elastic energy density are discussed.

DOI: 10.1103/PhysRevLett.125.248001

Advances in nanotechnology have revolutionized the capacity to fabricate nanoparticles (NPs) with exquisite control of their surface properties [1–3]. The broad design space spanned by surface modification and NP shape has enabled the fabrication of application-specific superstructures via assembly engineering strategies [4–8], including the use of charge-patterned NPs and electrostatic control [9–13]. Inspired by biology, there is a keen interest in how self-assembly is affected by building blocks that dynamically respond to stimuli and reconfigure during assembly [14–18]. This dynamic dimension enables unique structural organizations via otherwise inaccessible assembly pathways, broadening assembly engineering approaches to design reconfigurable materials [14,16]. For example, computational studies showed that shape-flexible nanorods could overcome kinetic barriers to yield reconfigurable structures that switch between assembled mesophases, such as square grids and bilayer sheets [14,19]. Additionally, phase transformations from simple cubic to rhombohedral structures were realized experimentally by accommodating the shape evolution of NPs from cubes to spheres [17].

Shape-changing NPs have also received attention as candidates for designing stimuli-responsive nanocontainers in therapeutic applications [20–22], where studies have demonstrated that the cellular uptake of nanocarriers is affected by their shape, size, charge, and deformability [21,23–25]. Many techniques have been developed to synthesize such nanostructures [2,26–28] utilizing different materials, including biomolecular constructs and polymer-based vesicles, where electrostatic interactions play a critical role in inducing shape changes via the control of *p*H or ionic strength [26,27,29,30].

Here, we address a class of dynamic nanoscale building blocks: deformable NPs whose surface is tailored with charged patches. Although utilization of rigid, patchy NPs is common in assembling desired structures, little is known regarding the utilization of spontaneous NP deformation based on the location, size, or the number of surface patches. Computational studies of deformations of patchy, flexible NPs have been largely limited to the use of elastic surface inhomogeneities, yielding, for example, regular polyhedra, buckled conformations, and collapsed bowl-like structures [31–33]. Alternatively, theoretical efforts have focused on understanding shape transitions in homogeneously charged nanostructures [34–37] and in uncharged elastic shells, whose deformation is driven by topological defects, compression, or magnetic forces [38–40]. Despite emerging capabilities for synthesizing charge-patterned NPs and colloids [3,41–43] and the prevalent use of electrostatic control to induce changes in material assembly behavior [13,44], a thorough understanding of the interplay between electrostatic and elastic energies for shape manipulation in charge-patterned flexible NPs is lacking [45].

We study a variety of shape-switching scenarios using a continuum model of deformable, hollow NPs to elucidate the relationship between surface charge patterns, deformability, and the low-energy shapes of NPs. We show that surface charge patterns can induce deformation in flexible NPs for a broad range of salt concentrations. Our simulations reveal that NPs with charged stripes, Janus patches, and polyhedrally distributed patches adapt their shape differently in response to changes in salt concentration over 0.05–20 mM, transforming into rodlike structures, capsules, spinning tops, hemispheres, variably dimpled bowls, and particles with polyhedral protrusions. These deformations, controlled by pattern type and screening length, can change the directional specificity of interactions between NPs, which may in turn hinder or promote reconfiguration in assembled materials. The charge-pattern-based shape control of deformable NPs revealed in this Letter has implications for the design of responsive nanocontainers and dynamic building blocks for assembling reconfigurable materials.

The model NPs are initialized as spherical containers of radius $R = 20$ nm. Bending modulus κ_b and stretching constant $\kappa_s = k_s R^2$, where k_s is the spring constant (proportional to the Young's modulus), are introduced to effectively account for the intermolecular short-range interactions that resist deformation. These 2D elastic parameters are chosen to be in a regime where the equilibrium shape without any surface charge is a sphere. The parameter values are inspired by experimental studies of soft hydrogel NP systems, which have a 3D Young's modulus in the range of 10–100 kPa and exhibit significant deformation [46–50]. Spontaneous buckling is suppressed by choosing a low Föppl–von Kármán number [38]. Long-range electrostatic interactions are included via a screened Coulomb potential with screening length λ representing the effects of mobile ions in solutions inhabiting the NP. The surface charge patterns are restricted to designed patches exhibiting charges of only one sign. The NP surface is discretized with N_v vertices, constituting N_e edges and N_f triangular faces. Using the discretization of the continuum expression for the elastic energy [51], the Hamiltonian $\mathcal{H}$ characterizing the NP system [34,36] is written in units of $k_B T$ as

$$\mathcal{H} = \frac{\kappa_b}{2}\sum_{l=1}^{N_e} |\vec{n}_{l_1} - \vec{n}_{l_2}|^2 + \frac{\kappa_s}{2R^2}\sum_{l=1}^{N_e}(|\vec{r}_{l_1} - \vec{r}_{l_2}| - a_l)^2 + \frac{l_B}{2}\sum_{i=1}^{i=N_v}\sum_{j\neq i}^{j=N_v} q_i q_j e^{-|\vec{r}_i - \vec{r}_j|/\lambda}/|\vec{r}_i - \vec{r}_j|, \quad (1)$$

where the first, second, and third term are the total bending, stretching, and electrostatic energy respectively. $\mathcal{H}$ is extended to include a volume constraint term, which allows NP volume changes on the order of 10% for shape deformations shown here (see Supplemental Material [52]). The choice of this volume constraint is inspired by experimental studies where preservation of the amount of cargo encapsulated within the NP is desired across different shapes [21,57]. In Eq. (1), $\vec{n}$ is the normal vector associated with a face, a_l is the equilibrium length of edge l, l_B is Bjerrum length in water, $\vec{r}_i$ denotes the position vector of vertex i, and q_i is the charge associated with this vertex.

To obtain the low-energy NP shapes, $\mathcal{H}$ is minimized subject to the volume constraint using a molecular dynamics (MD)-based simulated annealing procedure [34,36] accelerated with an OpenMP/MPI hybrid parallelization technique [58]. The low-energy NP shapes are controlled by the elastic moduli, charge pattern, and screening length. The effects of counterion condensation, which may lead to a reduction in the effective NP charge, are assessed by performing MD simulations of counterions near a NP with a shape produced via the energy minimization process [52]. These post-optimization simulations explicitly model the presence of counterions, including their interactions with the NP.

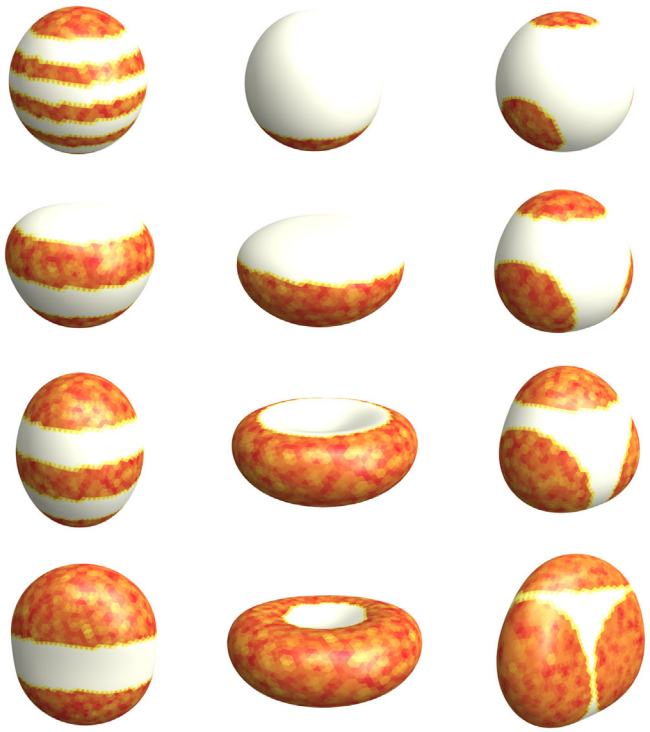

FIG. 1. Snapshots of low-energy shapes of deformable NPs for striped patterns (left column), Janus patches (middle column), and tetrahedrally distributed patches (right column). All NPs have initial volume $4/3\pi\ 20^3\ \mathrm{nm}^3$, with charged regions (orange) of charge density $0.12\ e/\mathrm{nm}^2$ in a salt solution at concentration 1 mM. Shifting the pattern changes the NP shape. Striped NPs form spherocylinders with rounded or flattened tops, Janus patches produce hemispheres and flattened bowls, and tetrahedrally distributed patches produce variably rounded tetrahedra.

Figure 1 shows the low-energy conformations of NPs for three distinct sets of designed surface charge patterns: alternating charged and neutral stripes of equal area, Janus patches with varying fractional surface charge coverage, and tetrahedrally distributed patches with varying patch size. For each set, the different patches have the same initial local charge density $\sigma = 0.12\ e/\mathrm{nm}^2$. All NPs are in an aqueous solution with salt concentration $c_s = 1$ mM and have elastic moduli of $\kappa_b = 5$ and $\kappa_s = 125$ (in units $k_B T$). NPs having striped patches yield spherocylinders including rodlike and capsule-shaped structures as the number of charged stripes is changed. Shapes with rounded or flattened ends are observed depending on the charged or neutral nature of the terminal ends. For Janus patches with fractional surface charge coverage p, the NP exhibits shape transitions from sphere ($p = 0$, fully uncharged) to hemisphere ($p = 0.5$) to variably dimpled bowls ($p = 0.75$, 0.9). NPs with charged patches centered around the sites of circumscribed tetrahedral vertices expand to generate variably rounded tetrahedral-shaped NPs, depending upon the patch size. For each of the three distinct types of charge patterns, as the uniformly charged limit is approached

(e.g., $p = 1$ for Janus patches), the low-energy shape converges to a disk conformation observed previously for uniformly charged deformable NPs [34–36].

For a given patterned NP, its shape can be further controlled by modifying solution conditions such as salt concentration c_s. The links between surface patterns and shapes associated with NPs under varying c_s can be presented in the form of two-dimensional contour plots using shape metrics such as asphericity. Figure 2(a) shows an asphericity shape map for NPs with Janus patches as a function of c_s and p [52]. The solution conditions and NP elastic properties are otherwise the same as in Fig. 1. The map is constructed via an interpolation of the data for the low-energy shapes generated from a set of 24 simulations of deformable NPs with $p = 0.25$, 0.5, 0.75, 0.9 and $c_s = 0.05$, 0.1, 0.5, 1, 5, 20 mM [52]. Asphericity contours demarcate regions of the design space capable of deforming NPs to a given extent. Other shape descriptors such as relative anisotropy yield similar results (see Supplemental Material [52]).

Figure 2(b) shows the changes in the total energy $\mathcal{H}$ and the area of the NP as a function of c_s for different Janus patches characterized with $p = 0.25$, 0.5, 0.75, 0.9. In all cases, the difference $\Delta\mathcal{H}$ between the total energy of the deformed NP and the undeformed (initial) NP is negative. The electrostatic and elastic energy components of $\mathcal{H}$ show that the NP lowers its electrostatic energy at the cost of an increase in its elastic energy and area [52]. Similar trends are observed for NPs with different patterns [52]. Figure 2(c) provides snapshots of a specific shape transition (from dimpled to flattened bowls) recorded in Figs. 2(a) and 2(b) for $p = 0.75$ as c_s is increased from 0.5 to 5 mM.

Figure 3 shows the distribution of local elastic energy density (sum of the bending and stretching energies) associated with a representative set of deformed NPs. The inhomogeneous elastic energy density exhibits a coupling to the anisotropic surface charge distribution in each case. For example, NPs with Janus patches exhibit a Janus-like elastic energy density, where an expansion of the charged regions of the NP results in a higher local elastic energy compared to the uncharged regions.

Charge anisotropy induces shape deformation, even for the case of low charge density σ with which NPs do not deform when the surface charge is uniformly distributed. We examined the shapes of NPs with Janus patches of $\sigma = 0.06\ e/\mathrm{nm}^2$ and elastic moduli approximately half of the values used in NPs studied in Fig. 1. When uniformly charged, the NP does not deform at $c_s = 1$ mM. However, generating an inhomogeneity in the form of an uncharged region induces deformation despite lowering the net surface charge (Fig. 4). Tuning the anisotropy of the surface charge deforms the NP into egglike, flattened bowl, and spinning-top shapes.

The charge density σ in the NP model implicitly includes the effects of charge renormalization due to ion condensation. All charged patches in Fig. 1 have the same $\sigma = 0.12\ e/\mathrm{nm}^2$. The NP surface charge, however, varies with the pattern and is largest ($\approx 600e$) for the homogeneously charged NP. MD simulations of monovalent counterions surrounding undeformed (spherical) NPs with

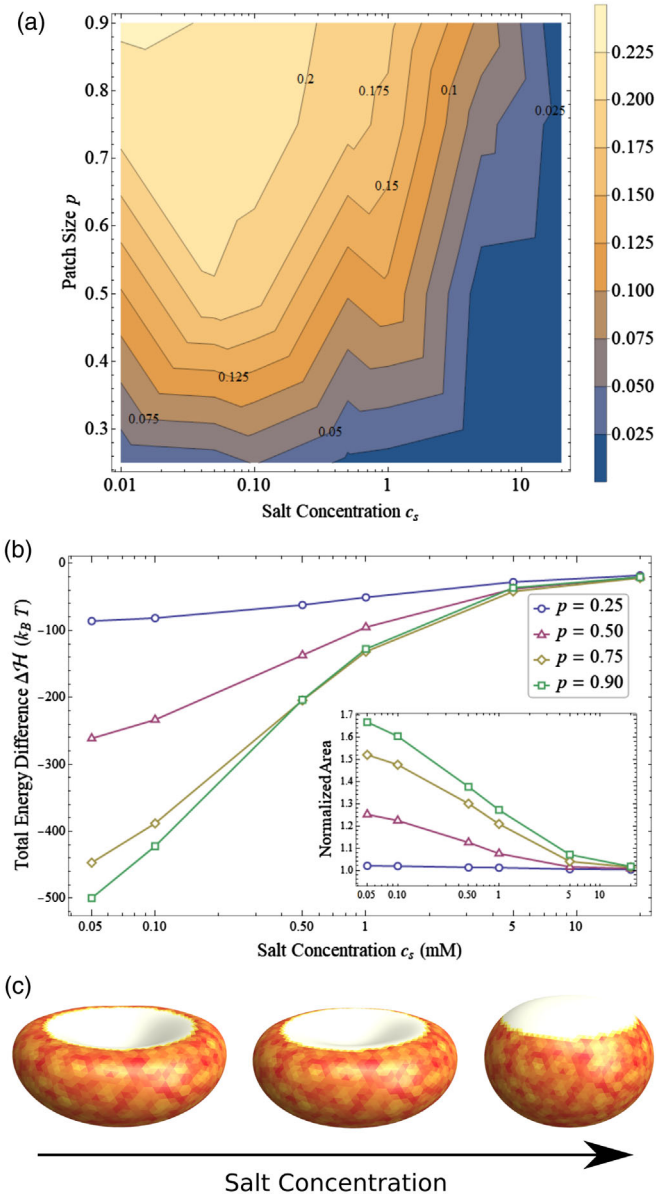

FIG. 2. Pattern-shape links analyzed for NPs patterned with Janus patches with fractional surface charge coverage $p \in (0.25, 0.9)$ (middle column in Fig. 1) for varying salt concentration $c_s \in (0.05, 20)$ mM. (a) Asphericity as a function of c_s and p. NPs associated with large p and small c_s exhibit higher asphericity, signaling greater deviations from the spherical conformation. (b) Changes in NP total energy and area (inset) vs c_s for different p. Shape transitions are accompanied by a decrease in the total energy and an increase in the area relative to the spherical conformation. (c) Representative snapshots of the low-energy shapes of Janus NPs with $p = 0.75$ as c_s increases from left to right.

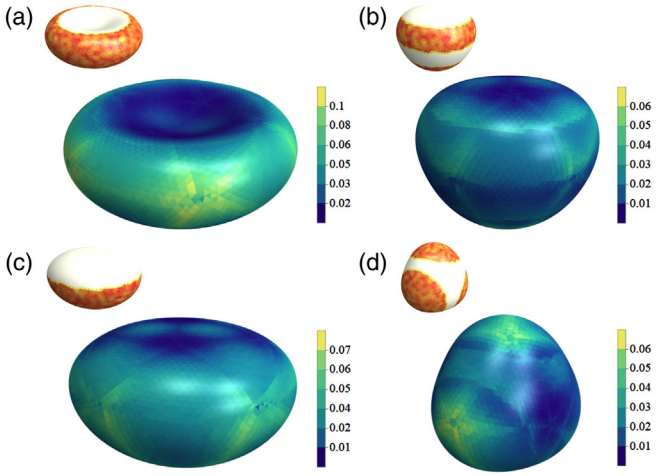

FIG. 3. The elastic energy distribution on the surface of the deformed NP for a representative set of NPs tailored with charge patterns shown in the top left. NPs with Janus patches characterized by fractional charge coverage $p = 0.75$ (a) and $p = 0.5$ (c) exhibit a Janus-like elastic energy density. A similar coupling between anisotropy in charge pattern and elastic energy density is observed in striped NPs (b) and NPs with polyhedrally distributed patches (d).

charge patterns depicted in Fig. 1 show that patchy NPs experience less ion condensation compared to homogeneously charged NPs. For example, in the case of undeformed NPs with Janus patches characterized with patch size p, the majority of counterions condense on the charged portion of the NP, which reduces the effective local charge density to $\approx 0.09\ e/\mathrm{nm}^2$ for low $p = 0.25$ and down to $\approx 0.05\ e/\mathrm{nm}^2$ for high $p = 1$ (Supplemental Material [52]). NPs with other patterns exhibit similar trends. As condensation effects are most severe for the uniformly charged spherical NP, the latter can be used to assess the feasibility of realizing a charge density of $0.12\ e/\mathrm{nm}^2$ in the event of ion condensation, which is known to limit the maximum effective charge or the critical valence [59]. The extent to which ion condensation lowers the critical valence is dependent on NP packing fraction η and c_s. Mean-field calculations based on the Manning model [34–36,52,60] show that uniformly charged spherical NPs under salt-free conditions have a critical valence greater than $\sigma = 0.12\ e/\mathrm{nm}^2$ for $\eta < 10^{-8}$. By the above arguments, this σ value is also feasible for charge-patterned NPs for similarly low η.

For high NP packing fraction, the σ value in the coarse-grained model needs to be lowered as stronger condensation effects are expected [36,59]. MD simulations of counterions surrounding NPs characterized with Janus-like patches of size p and bare charge density $\sigma_b = 0.12\ e/\mathrm{nm}^2$ show significant condensation at $\eta = 10^{-2}$ for both undeformed and deformed NPs shown in Fig. 1 [52]. The associated effective charge reduces from $150e$ to $\approx 120e$ for $p = 0.25$ and from $600e$ to $\approx 220e$ for $p = 1$. The condensation effects are most severe for the homogeneously charged ($p = 1$) NPs that yield disklike structures, for which calculations are analytically tractable [34,36,52]. A Manning two-state model can be used to analyze the condensation effects under salt-free conditions for different packing fractions η [52]. The model approximately reproduces the effective charge ($\approx 220e$) estimated by the explicit-ion MD simulations at $\eta = 10^{-2}$ for $p = 1$. Using the model, we compute the effective charge and the free energy for $\eta \in (10^{-12}, 10^{-2})$, where the latter comprises the electrostatic free energy and the NP elastic energy. The difference in the net free energy of a disk-shaped NP of aspect ratio ≈ 0.3 (produced in our simulations for $p = 1$) relative to that of a sphere, remains negative by over $\approx 100 k_B T$ for $10^{-12} < \eta < 10^{-4}$ (Fig. 5 in the Supplemental Material [52]). The free-energetic drive to deform can be further enhanced for reduced effective charges by synthesizing less rigid NPs. For example, deformations similar to those observed for NPs with Janus patches (Fig. 1) are achieved with lower $\sigma = 0.09\ e/\mathrm{nm}^2$ for NPs with reduced elastic parameters: $\kappa_b = 3$ and $\kappa_s = 75$ [52].

We also note that the difference in the extent of ion liberation between spherical and deformed patterned NPs is small for all patterns, as indicated by the slight increase in the effective charges of deformed NPs extracted via MD simulations (Fig. 4 in the Supplemental Material [52]). We thus do not expect ion release and associated entropic effects to sufficiently counteract the electrostatic drive to deform, as has been found for highly charged nanocontainers [59]. However, the effects of explicit counterion-NP interactions during the shape change process are neglected in our model. A dramatic reduction in the ion condensation during the shape change process may result in an increase in the free energy of the released counterions, stabilizing the spherical shape [59]. These effects may

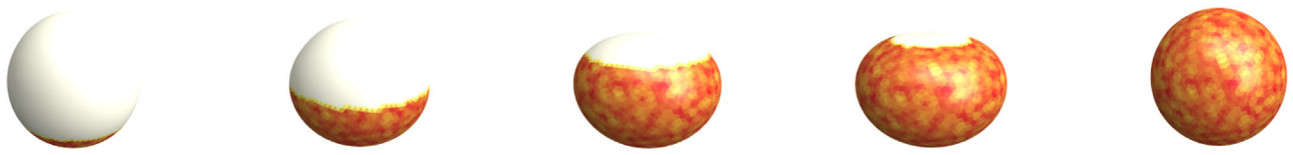

FIG. 4. Low-energy shapes of NPs with Janus patches of charge density $\sigma = 0.06\ e/\mathrm{nm}^2$ and elastic moduli $\kappa_b = 3$ and $\kappa_s = 75$ (in units of $k_B T$). Patch size increases from left to right as $p = 0.25, 0.50, 0.75, 0.90, 1.0$; other parameters are the same as in Fig. 1. Anisotropy of the surface charge itself causes deformation; when uniformly charged ($p = 1$), the NP does not deform.

affect the parameter regimes to realize shape transitions, in particular, for high packing fractions.

We have demonstrated the capacity to electrostatically control the shape of hollow, deformable NPs via the synthesis of surface charge patterns. Our simulations showed that NPs with Janus patches, stripes, and polyhedrally distributed patches adapt their shape in response to changes in solution conditions and pattern tuning, transforming into different structures including spherocylinders, spinning tops, hemispheres, bowls, and polyhedral particles. The model can be readily extended to address other charge patterns, including oppositely charged patches, and particles of larger size [36]. Our initial studies indicate larger NPs of radius 100 nm with the same charge density and smaller Young's modulus (within the 10–100 kPa range) deform into shapes similar to those shown in Fig. 1. However, we expect transitions to become less feasible for much larger particles (radius $\gtrsim 10$ μm) as the elastic modulus and salt concentration enabling deformation may become prohibitively low. A key experimental challenge will be to synthesize deformable NPs with tailored charge patterns. Phase separation and masking techniques are established methods for synthesizing polymer-based patchy particles [43], which may be utilized with *p*H-responsive polymers to form charge-patterned NPs [2,43]. Further, methods of controlling the extent of cross-linking in polymeric NPs [46,50] can enable the tuning of their elasticities to facilitate the deformation of charge-patterned NPs within the range of solution conditions explored in this Letter.

This work is supported by the NSF through Grants No. DMR-1753182 and No. 1720625. Simulations were performed using the Big Red supercomputing systems.

*vjadhao@iu.edu

[1] J. A Champion, Y. K Katare, and S. Mitragotri, Making polymeric micro-and nanoparticles of complex shapes, Proc. Natl. Acad. Sci. U.S.A. **104**, 11901 (2007).

[2] D. Klinger, C. X. Wang, L. A. Connal, D. J. Audus, S. G. Jang, S. Kraemer, K. L. Killops, G. H. Fredrickson, E. J. Kramer, and C. J. Hawker, A facile synthesis of dynamic, shape-changing polymer particles, Angew. Chem., Int. Ed. Engl. **53**, 7018 (2014).

[3] P. D. J. van Oostrum, M. Hejazifar, C. Niedermayer, and E. Reimhult, Simple method for the synthesis of inverse patchy colloids, J. Phys. Condens. Matter **27**, 234105 (2015).

[4] P. Akcora, H. Liu, S. K. Kumar, J. Moll, Y. Li, B. C. Benicewicz, L. S. Schadler, D. Acehan, A. Z. Panagiotopoulos, V. Pryamitsyn *et al.*, Anisotropic self-assembly of spherical polymer-grafted nanoparticles, Nat. Mater. **8**, 354 (2009).

[5] D. J. Kraft, R. Ni, F. Smallenburg, M. Hermes, K. Yoon, D. A. Weitz, A. van Blaaderen, J. Groenewold, M. Dijkstra, and W. K. Kegel, Surface roughness directed self-assembly of patchy particles into colloidal micelles, Proc. Natl. Acad. Sci. U.S.A. **109**, 10787 (2012).

[6] S. C. Glotzer, Assembly engineering: Materials design for the 21st century (2013 P. V. Danckwerts lecture), 2013 Danckwerts Special Issue on Molecular Modelling in Chemical Engineering, Chem. Eng. Sci. **121**, 3 (2015).

[7] L. Rossi, V. Soni, D. J. Ashton, D. J. Pine, A. P. Philipse, P. M. Chaikin, M. Dijkstra, S. Sacanna, and W. T. M. Irvine, Shape-sensitive crystallization in colloidal superball fluids, Proc. Natl. Acad. Sci. U.S.A. **112**, 5286 (2015).

[8] A. Reddy, M. B. Buckley, A. Arora, F. S. Bates, K. D. Dorfman, and G. M. Grason, Stable Frank–Kasper phases of self-assembled, soft matter spheres, Proc. Natl. Acad. Sci. U.S.A. **115**, 10233 (2018).

[9] R. M. Adar, D. Andelman, and H. Diamant, Electrostatics of patchy surfaces, Adv. Colloid Interface Sci. **247**, 198 (2017).

[10] B. Luo, J. W. Smith, Z. Wu, J. Kim, Z. Ou, and Q. Chen, Polymerization-like co-assembly of silver nanoplates and patchy spheres, ACS Nano **11**, 7626 (2017).

[11] S. Gangwal, A. Pawar, I. Kretzschmar, and O. D. Velev, Programmed assembly of metallodielectric patchy particles in external ac electric fields, Soft Matter **6**, 1413 (2010).

[12] J. M. Dempster and M. Olvera de la Cruz, Aggregation of heterogeneously charged colloids, ACS Nano **10**, 5909 (2016).

[13] C. Gao, S. Kewalramani, D. Maria Valencia, H. Li, J. M. McCourt, M. Olvera De La Cruz, and M. J. Bedzyk, Electrostatic shape control of a charged molecular membrane from ribbon to scroll, Proc. Natl. Acad. Sci. U.S.A. **116**, 22030 (2019).

[14] T. Dac Nguyen, E. Jankowski, and S. C. Glotzer, Self-assembly and reconfigurability of shape-shifting particles, ACS Nano **5**, 8892 (2011).

[15] V. M. O. Batista and M. A. Miller, Crystallization of Deformable Spherical Colloids, Phys. Rev. Lett. **105**, 088305 (2010).

[16] O. Gang and Y. Zhang, Shaping phases by phasing shapes, ACS Nano **5**, 8459 (2011).

[17] Y. Zhang, F. Lu, D. van der Lelie, and O. Gang, Continuous Phase Transformation in Nanocube Assemblies, Phys. Rev. Lett. **107**, 135701 (2011).

[18] K. Bian, J. J. Choi, A. Kaushik, P. Clancy, D.-M. Smilgies, and T. Hanrath, Shape-anisotropy driven symmetry transformations in nanocrystal superlattice polymorphs, ACS Nano **5**, 2815 (2011).

[19] T. Dac Nguyen and S. C. Glotzer, Reconfigurable assemblies of shape-changing nanorods, ACS Nano **4**, 2585 (2010).

[20] N. S. Abadeer and C. J. Murphy, Recent progress in cancer thermal therapy using gold nanoparticles, J. Phys. Chem. C **120**, 4691 (2016).

[21] Y. Liu, J. Tan, A. Thomas, D. Ou-Yang, and V. R. Muzykantov, The shape of things to come: Importance of design in nanotechnology for drug delivery, Ther. Delivery **3**, 181 (2012).

[22] K. Zhou, Y. Wang, X. Huang, K. Luby-Phelps, B. D. Sumer, and J. Gao, Tunable, ultrasensitive ph-responsive nanoparticles targeting specific endocytic organelles in living cells, Angew. Chem., Int. Ed. Engl. **50**, 6109 (2011).

[23] N. Shimokawa, H. Ito, and Y. Higuchi, Coarse-grained molecular dynamics simulation for uptake of nanoparticles into a charged lipid vesicle dominated by electrostatic interactions, Phys. Rev. E **100**, 012407 (2019).
[24] D. B. Chithrani, Intracellular uptake, transport, and processing of gold nanostructures, Molecular membrane biology **27**, 299 (2010).
[25] S. Nangia and R. Sureshkumar, Effects of nanoparticle charge and shape anisotropy on translocation through cell membranes, Langmuir **28**, 17666 (2012).
[26] A. P. Blum, J. K. Kammeyer, A. M. Rush, C. E. Callmann, M. E. Hahn, and N. C. Gianneschi, Stimuli-responsive nanomaterials for biomedical applications, J. Am. Chem. Soc. **137**, 2140 (2015).
[27] J.-W. Yoo and S. Mitragotri, Polymer particles that switch shape in response to a stimulus, Proc. Natl. Acad. Sci. U.S.A. **107**, 11205 (2010).
[28] J.-M. Williford, Y. Ren, K. Huang, D. Pan, and H.-Q. Mao, Shape transformation following reduction-sensitive PEG cleavage of polymer/DNA nanoparticles, J. Mater. Chem. B **2**, 8106 (2014).
[29] F. Checot, S. Lecommandoux, H.-A. Klok, and Y. Gnanou, From supramolecular polymersomes to stimuli-responsive nano-capsules based on poly (diene-b-peptide) diblock copolymers, Eur. Phys. J. E **10**, 25 (2003).
[30] K. E. Gebhardt, S. Ahn, G. Venkatachalam, and D. A. Savin, Rod-sphere transition in polybutadiene- poly (l-lysine) block copolymer assemblies, Langmuir **23**, 2851 (2007).
[31] G. Vernizzi, R. Sknepnek, and M. Olvera de la Cruz, Platonic and archimedean geometries in multicomponent elastic membranes, Proc. Natl. Acad. Sci. U.S.A. **108**, 4292 (2011).
[32] J. Paulose and D. R. Nelson, Buckling pathways in spherical shells with soft spots, Soft Matter **9**, 8227 (2013).
[33] R. Sknepnek and M. Olvera de la Cruz, Nonlinear elastic model for faceting of vesicles with soft grain boundaries, Phys. Rev. E **85**, 050501(R) (2012).
[34] V. Jadhao, C. K. Thomas, and M. Olvera de la Cruz, Electrostatics-driven shape transitions in soft shells, Proc. Natl. Acad. Sci. U.S.A. **111**, 12673 (2014).
[35] V. Jadhao, Z. Yao, C. K. Thomas, and M. Olvera De La Cruz, Coulomb energy of uniformly charged spheroidal shell systems, Phys. Rev. E **91**, 032305 (2015).
[36] N. E. Brunk and V. Jadhao, Computational studies of shape control of charged deformable nanocontainers, J. Mater. Chem. B **7**, 6370 (2019).
[37] Z. Yao and M. Olvera De La Cruz, Electrostatics-Driven Hierarchical Buckling of Charged Flexible Ribbons, Phys. Rev. Lett. **116**, 148101 (2016).
[38] J. Lidmar, L. Mirny, and D. R. Nelson, Virus shapes and buckling transitions in spherical shells, Phys. Rev. E **68**, 051910 (2003).
[39] G. A. Vliegenthart and G. Gompper, Compression, crumpling and collapse of spherical shells and capsules, New J. Phys. **13**, 045020 (2011).
[40] H. Yuan and M. Olvera de la Cruz, Crystalline membrane morphology beyond polyhedra, Phys. Rev. E **100**, 012610 (2019).
[41] F. Chang, B. G. P. Van Ravensteijn, K. S. Lacina, and W. K. Kegel, Bifunctional Janus spheres with chemically orthogonal patches, ACS Macro Lett. **8**, 714 (2019).
[42] Y. Yi, L. Sanchez, Y. Gao, and Y. Yu, Janus particles for biological imaging and sensing, Analyst **141**, 3526 (2016).
[43] M. Lattuada and T. A. Hatton, Synthesis, properties and applications of Janus nanoparticles, Nano Today **6**, 286 (2011).
[44] N. E. Brunk, M. Uchida, B. Lee, M. Fukuto, L. Yang, T. Douglas, and V. Jadhao, Linker-mediated assembly of virus-like particles into ordered arrays via electrostatic control, ACS Appl. Bio Mater. **2**, 2192 (2019).
[45] R. Sknepnek, G. Vernizzi, and M. Olvera de la Cruz, Shape Change of Nanocontainers via a Reversible Ionic Buckling, Phys. Rev. Lett. **106**, 215504 (2011).
[46] J. W. Myerson, B. Braender, O. Mcpherson, P. M. Glassman, R. Y. Kiseleva, V. V. Shuvaev, O. Marcos-Contreras, M. E. Grady, H.-S. Lee, C. F. Greineder *et al.*, Flexible nanoparticles reach sterically obscured endothelial targets inaccessible to rigid nanoparticles, Adv. Mater. **30**, 1802373 (2018).
[47] C. Huang, P. J. Butler, S. Tong, H. S. Muddana, G. Bao, and S. Zhang, Substrate stiffness regulates cellular uptake of nanoparticles, Nano Lett. **13**, 1611 (2013).
[48] S. Zhang, H. Gao, and G. Bao, Physical principles of nanoparticle cellular endocytosis, ACS Nano **9**, 8655 (2015).
[49] P. Guo, D. Liu, K. Subramanyam, B. Wang, J. Yang, J. Huang, D. T. Auguste, and M. A. Moses, Nanoparticle elasticity directs tumor uptake, Nat. Commun. **9**, 130 (2018).
[50] X. Banquy, F. Suarez, A. Argaw, J.-M. Rabanel, P. Grutter, J.-F. Bouchard, P. Hildgen, and S. Giasson, Effect of mechanical properties of hydrogel nanoparticles on macrophage cell uptake, Soft Matter **5**, 3984 (2009).
[51] H. S. Seung and D. R. Nelson, Defects in flexible membranes with crystalline order, Phys. Rev. A **38**, 1005 (1988).
[52] See Supplemental Material at http://link.aps.org/supplemental/10.1103/PhysRevLett.125.248001 for details of the model, simulation methods, shape descriptors, and ion condensation effects, which includes Refs. [53–56].
[53] *Wolfram Research, Inc., Mathematica, Version 12.1* (Wolfram Research, Inc., Champaign, 2020).
[54] S. Plimpton, Fast parallel algorithms for short-range molecular dynamics, J. Comput. Phys. **117**, 1 (1995).
[55] A. Diehl and Y. Levin, Effective charge of colloidal particles, J. Chem. Phys. **121**, 12100 (2004).
[56] H. Arkın and W. Janke, Gyration tensor based analysis of the shapes of polymer chains in an attractive spherical cage, J. Chem. Phys. **138**, 054904 (2013).
[57] S. E. A. Gratton, P. A. Ropp, P. D. Pohlhaus, J. C. Luft, V. J. Madden, M. E. Napier, and J. M. DeSimone, The effect of particle design on cellular internalization pathways, Proc. Natl. Acad. Sci. U.S.A. **105**, 11613 (2008).
[58] Code available at https://github.com/softmaterialslab/np-shape-lab/.
[59] Y. S. Jho, J. Landy, and P. A. Pincus, Charge renormalization for ellipsoidal macroions, ACS Macro Lett. **4**, 640 (2015).
[60] G. S. Manning, Counterion condensation on charged spheres, cylinders, and planes, J. Phys. Chem. B **111**, 8554 (2007).